A comprehensive evaluation of factors that influence the spin polarization of electrons emitted from bulk GaAs photocathodes

Wei Liu, Matt Poelker, Xincun Peng, Shukui Zhang, and Marcy Stutzman

Citation: Journal of Applied Physics **122**, 035703 (2017); doi: 10.1063/1.4994306
View online: http://dx.doi.org/10.1063/1.4994306
View Table of Contents: http://aip.scitation.org/toc/jap/122/3
Published by the American Institute of Physics

A comprehensive evaluation of factors that influence the spin polarization of electrons emitted from bulk GaAs photocathodes

Wei Liu,[1,2,3] Matt Poelker,[3] Xincun Peng,[3,4] Shukui Zhang,[3] and Marcy Stutzman[3]
[1]*Institute of Modern physics, Chinese Academy of Sciences, 509 Nanchang Rd., Lanzhou 730000, China*
[2]*University of Chinese Academy of Sciences, 19A Yuquan Rd., Beijing 100049, China*
[3]*Thomas Jefferson National Accelerator Facility, 12000 Jefferson Avenue, Newport News, Virginia 23606, USA*
[4]*Engineering Research Center of New Energy Technology of Jiangxi Province, East China Institute of Technology, Nanchang 330013, China*

(Received 6 March 2017; accepted 5 July 2017; published online 19 July 2017)

The degree of polarization of photoemitted electrons extracted from bulk unstrained GaAs photocathodes is usually considerably less than the theoretical maximum value of 50%, as a result of depolarization mechanisms that originate within the photocathode material and at the vacuum surface interface. This paper provides a comprehensive review of depolarization mechanisms and presents a systematic experimental evaluation of polarization sensitivities to temperature, dopant density, quantum efficiency, and crystal orientation. The highest measured polarization was ~50%, consistent with the maximum theoretical value, obtained from a photocathode sample with relatively low dopant concentration and cooled to 77 K. In general, measurements indicate electron spin polarization can be enhanced at the expense of photoelectron yield (or quantum efficiency). *Published by AIP Publishing.* [http://dx.doi.org/10.1063/1.4994306]

I. INTRODUCTION

Photoelectron yield, or quantum efficiency (QE), and electron spin polarization (ESP) are important characteristics of GaAs photocathodes used at electron accelerators worldwide. For decades, photocathode experts have worked to increase these quantities. The QE of GaAs photocathodes is affected by many factors, including cathode material quality, the wavelength of the incident light, the thickness of the photocathode, dopant density, the temperature of the photocathode, surface contamination, the negative electron affinity (NEA) condition on the photocathode surface, the power density of the laser light, the bias voltage, and the vacuum pressure under which photo-extracted beam is produced. These factors also affect ESP via spin relaxation/depolarization mechanisms that influence conduction-band electrons migrating toward the surface of the photocathode, and then emitted into vacuum. Although bulk GaAs provides relatively low polarization compared to the strained-superlattice photocathodes commonly used at modern polarized electron accelerators,[1–3] it represents a convenient and inexpensive tool that can help differentiate depolarization mechanisms and possibly assist with the engineering of higher polarization photocathodes by providing benchmarks for proposed Monte Carlo simulations aimed at modeling polarized photoemission.[4] And because high polarization strained-superlattice photocathodes possess relatively low QE, bulk GaAs—with higher QE—might be the only photocathode material that can satisfy the high current requirements of some proposed new applications.[5,6] This work provides an updated evaluation of polarization sensitivities of bulk unstrained GaAs.

GaAs is a direct-transition III-V semiconductor with zincblende crystal structure. It can absorb laser light across the broad visible spectrum, but only illumination with near-IR wavelengths provides polarized photoemission. This can be understood by looking at detailed[7] and simplified[8] representations of the energy level diagrams of GaAs. Electron spin-orbit coupling splits the $P_{1/2}$ and $P_{3/2}$ energy levels of the valence band into two states separated by 0.33 eV, which is large enough to avoid optical pumping from the lower energy $P_{1/2}$ state. Polarized photoemission takes advantage of the quantum mechanical selection rules, noting that for circularly polarized laser light, conservation of angular momentum requires an electron's spin-angular momentum quantum number to change by one unit, $\Delta m_j = \pm 1$. Furthermore, some transitions are more favorable than others as indicated by the relative transition strengths shown in Fig. 1 (right). By using circularly polarized laser light with near-bandgap energy, the conduction band can be preferentially populated with a particular spin state. Polarization is defined as $P = \frac{N\uparrow - N\downarrow}{N\uparrow + N\downarrow}$, where N refers to the number of electrons in the conduction band of each spin state, "up" or "down." For bulk GaAs, the theoretical maximum polarization is 50%, corresponding to three electrons of the desired spin state for every one electron with opposite spin.

The emission of electrons from GaAs is often described as a three-step process,[9] involving absorption of light, diffusion of electrons to the surface of the photocathode, and emission of the electrons into the gun vacuum chamber. As described earlier, absorption of circularly polarized light with near-band gap energy preferentially populates the conduction band with spin polarized electrons. GaAs is a strong absorber with most of the light absorbed within a few hundred nanometers. These electrons diffuse in all directions and those that move toward the surface encounter a potential barrier known as the electron affinity (*EA* in Fig. 2). A requirement for efficient photoemission is that the GaAs be p-doped,[10] which serves to lower the Fermi level throughout

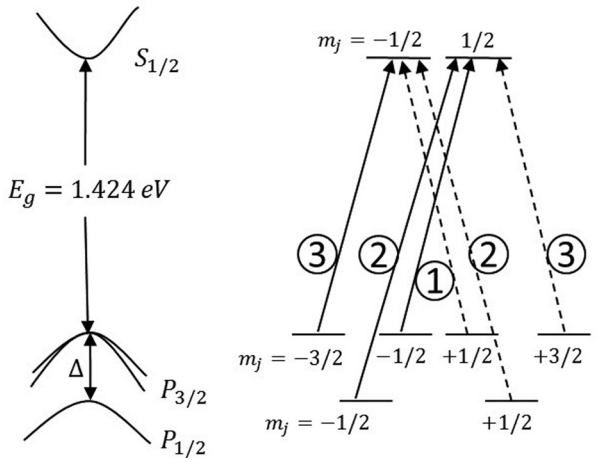

FIG. 1. (Left) Energy level diagram of GaAs at the center of the Brillouin zone: a "close-up" view near the valance band maxima/conduction band minima, and (right) simplified view showing the optical transitions between sublevels for right circularly polarized light (solid lines) and left circularly polarized light (dashed lines), with relative transition strengths given by circled numbers.

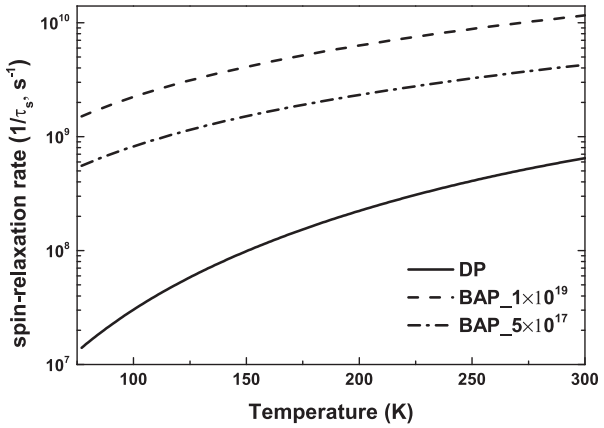

FIG. 3. Temperature dependence of the spin relaxation rate for DP and BAP mechanism in bulk GaAs with dopant concentration of 5×10^{17} cm^{-3} and 1×10^{19} cm^{-3}.

the material. The p-dopant also serves to lower the conduction band at the surface of the photocathode, which in turn lowers the electron affinity [EA_{eff} in Fig. 3(b)]. Still, no significant photoemission is obtained until the potential barrier is reduced further and this is accomplished by adding a few monoatomic layer of cesium and oxidant [Fig. 3(c)]. The process of adding cesium and oxidant to the photocathode surface is called "activation." In this work, fluorine served as the oxidant.

At room temperature, highly doped bulk GaAs photocathodes typically provide ESP of the order ∼30%, a value considerably less than the theoretical maximum value of 50%. The investigation of spin relaxation and depolarization has a long history dating back to the 1950s. Literature describes two main spin relaxation mechanisms for p-type III-V semiconductors: (1) the lack of inversion symmetry in III-V semiconductor leads to a spin splitting of the conduction band, called the D'yakonov-Perel (DP) mechanism,[11] and (2) the exchange interaction between electrons and holes, called the Bir-Aronov-Pikus (BAP) mechanism.[12] As described below, for p-type GaAs, the BAP mechanism dominates with the DP mechanism playing a role at high temperature and low dopant concentration.[13,14] There are other depolarization processes, but these are typically considered to have little consequence and are frequently ignored. These include the Elliot-Yafet (EY) mechanism[15,16] in which the spin–orbit interaction generates non-pure spin states in the conduction band, and radiation trapping, in which ESP is diluted by supplemental photoemission that results from the absorption of linearly polarized recombination light. There is a wealth of literature describing polarization studies using bulk GaAs, as a function of temperature,[17–19] dopant concentration,[17–19] electron (and hole) density,[20] and thickness of the photocathode.[21] In this paper, we revisit some of these studies using commercial bulk GaAs samples and modern equipment and vacuum techniques, evaluating ESP sensitivity to sample temperature, Zn dopant density, Cs-F activation layer, and surface cleave plane orientation. The sample temperature, dopant density, and the surface NEA layer have a significant impact on ESP, whereas ESP is insensitive to cleave plane orientation. In general, ESP can be increased at the expense of QE. The highest polarization of 50% was

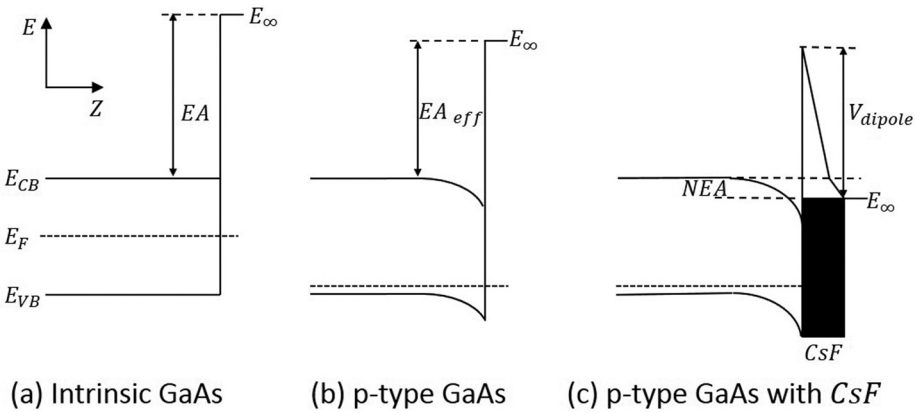

FIG. 2. Energy level diagrams describing the formation of the negative electron affinity (NEA) condition on GaAs. E_{cb}, E_F, E_{vb}, and E_∞ describe the conduction band energy, the fermi level, the valance band energy, and the vacuum energy level, respectively. EA and EA_{eff} refer to the electron affinity which is related to the surface work function. V_{dipole} is the decrease of vacuum level caused by the activation layer (Cs-F). (a) Intrinsic GaAs (b) p-type dopant lowers the Fermi level which leads to band bending at the surface (c) adding a Cs-F layer lowers the surface potential barrier and leads to further band bending.

obtained using a bulk GaAs photocathode at 77 K and with a relatively low dopant density.

II. THEORY

A. Spin relaxation mechanism

Electrons in the conduction band will arrive at an equilibrium polarization when the photocathode reaches a steady-state condition defined as $dP/dt = P_0/\tau - P/\tau - P/\tau_s = 0$. The term P_0/τ is the rate of polarization creation using circularly polarized light, P/τ describes polarization loss due to electron recombination to the valence band, and P/τ_s is the rate at which polarization disappears due to spin relaxation effects. So, the equilibrium polarization is given by[17]

$$P = P_0 \frac{1}{1 + \frac{\tau}{\tau_s}}, \tag{1}$$

where P_0 is the initial polarization determined by the quantum mechanical selection rules (as mentioned above, $P_0 = 50\%$ for bulk GaAs), τ and τ_s describe the electron lifetime and spin relaxation time for electrons at the bottom of the conduction band, respectively. The electron lifetime τ of GaAs is of the order 10^{-9} to 10^{-10} s, with the exact value dependent on the temperature and doping concentration of the sample. The cumulative spin relaxation rate is composed of individual spin relaxation mechanisms given by $1/\tau_s = 1/\tau_s^{DP} + 1/\tau_s^{BAP} + 1/\tau_s^{EY} + 1/\tau_s^{rad}$, where the superscripts represent the different spin relaxation mechanisms mentioned earlier. For p-type GaAs, the terms related to the EY mechanism and radiation trapping can be neglected.

The lack of inversion symmetry in GaAs is due to the presence of two distinct atoms in the Bravais lattice, such that the spin-up and spin-down electrons are not degenerate: $E_{k\uparrow} \neq E_{k\downarrow}$. The resulting energy difference plays the role of an effective magnetic field and results in spin precession during the time between collisions, which contributes to spin relaxation because the magnitude and direction of $\vec{k}$ changes in an uncontrolled way. This is the so called DP mechanism, and the spin relaxation rate is given by[11,22]

$$\frac{1}{\tau_s^{DP}} = Q\tau_p \alpha_0^2 \frac{(k_B T)^3}{\hbar^2 E_g}, \tag{2}$$

where Q is a dimensionless factor and ranges from 0.8 to 2.7 depending on the dominant momentum scattering mechanism, τ_p is the momentum relaxation time, α_0 is a dimensionless parameter specifying the strength of the spin-orbit interaction $\left(\alpha_0 = 4m_e\Delta/m_{ev}\left((E_g+\Delta)(3E_g+2\Delta)\right)^{\frac{1}{2}}\right.$, where Δ is the spin-orbit splitting of the valence band, m_e is the effective mass of the electron, and m_{ev} is a constant close in magnitude to the mass of the free electron[18]), and E_g is the bandgap of GaAs. The temperature dependence of the spin relaxation rate is $1/\tau_s^{DP} \sim T^3\tau_p \sim T^{9/2}$.[18]

In p-type GaAs, spin relaxation can result from the spin exchange interaction between electrons and holes. This is the so-called BAP mechanism, and the spin relaxation rate is given by two terms.[12,22] In case of exchange with nondegenerate holes

$$\frac{1}{\tau_s^{BAP}} = \frac{2}{\tau_0} N_A a_B^3 \frac{v_k}{v_B}\left[\frac{N_h}{N_A}|\psi(0)|^4 + \frac{5}{3}\frac{N_A - N_h}{N_A}\right], \tag{3}$$

where τ_0 is an exchange splitting parameter given by $1/\tau_0 = (3\pi/64)\Delta_{ex}^2/\hbar E_B$ (with Δ_{ex} is the exchange splitting of the excitonic ground state and $E_B = \hbar^2/2m_e a_B^2$ is the Bohr exciton energy), $a_B = \hbar^2\epsilon/e^2 m_e$ is the Bohr exciton radius, v_k is the electron velocity, $v_B = \hbar/m_e a_B$ is the Bohr exciton velocity, N_h is the density of free holes, N_A is the acceptor number density, and $|\psi(0)|^2$ is the Sommerfeld's factor.

In the case of exchange with degenerate holes and when the electron velocity v_k is greater than the Fermi velocity of the holes, the spin relaxation rate is given by[22]

$$\frac{1}{\tau_s^{BAP}} = \frac{3}{\tau_0} N_h a_B^3 \frac{v_k}{v_B}\frac{k_B T}{E_f}, \tag{4}$$

where E_f is the hole Fermi energy. If the electrons are thermalized, v_k needs to be replaced by the thermal velocity $v_e = (3k_B T/m_e)^{1/2}$.

The temperature dependence of τ_s^{BAP} is dominated by the temperature dependence of $|\psi(0)|^2$ as well as by the density of free holes N_h. The dependence on the acceptor density is essentially $1/\tau_s^{BAP} \sim N_A$ for nondegenerate holes from Eq. (3) and $1/\tau_s^{BAP} \sim N_A^{1/3}$ for degenerate holes from Eq. (4). In this paper, measurements of ESP as a function of sample temperature and dopant density serve to validate these assumptions.

The formulas cited earlier [Eqs. (2)–(4)] were used to calculate the spin relaxation rate as a function of temperature for bulk GaAs with dopant concentrations $1 \times 10^{19}\,\mathrm{cm}^{-3}$ and $5 \times 10^{17}\,\mathrm{cm}^{-3}$, as shown in Fig. 3. The BAP mechanism clearly dominates over the DP mechanism that contributes appreciably only at a higher temperature. The clear message from this plot is that low spin relaxation rates—and therefore higher ESP—will be obtained at lower dopant densities and temperatures. For the p-doped samples evaluated in this work and over the temperature range studied, the spin relaxation rate $1/\tau_s$ varied from $\sim 6 \times 10^8$ to $1 \times 10^{10}\,\mathrm{s}^{-1}$, corresponding to spin relaxation times between 10^{-10}–10^{-9} s.

B. Evaluation of electron escape probability

The QE of a GaAs photocathode can be estimated by[23]

$$QE = (1-R)\frac{P_{esc}}{1 + \frac{1}{\alpha L}}, \tag{5}$$

where R represents the reflectively of the photocathode, α is the absorption coefficient, L describes the electron diffusion length, and P_{esc} is the electron escape probability. Since the QE of a photocathode is easily measured as a function of the illumination wavelength, Eq. (5) can be used to solve for the escape probability, which is expected to be very sensitive to the photocathode surface condition and activation process, and

therefore could prove relevant for interpreting polarization behavior. Rewriting Eq. (5) to solve for P_{esc} yields

$$P_{esc} = \left(1 + \frac{1}{\alpha L}\right)\frac{QE}{(1-R)}. \tag{6}$$

The reflectivity R and the absorption coefficient α depend on the wavelength of incident light and the temperature of the photocathode, whereas the electron diffusion length L depends on the temperature and doping concentration of the sample. Values at room temperature can be found in literature, but in sections below, expressions are developed to estimate these terms at any temperature.

1. Modeling the optical constants R and α of GaAs

The optical dielectric function $\epsilon = \epsilon_1 + i\epsilon_2 = \overline{n}^2 = (n + ik)^2$ is estimated by the modified Adachi's model. The optical dielectric function in Adachi's model[24,25] is represented by the sum of terms attributed to four energy gaps (E_0, $E_0 + \Delta_0$, E_1, $E_1 + \Delta_1$) and damped harmonic oscillators describing the contributions from higher lying transitions (E_0', $E_2(X)$, $E_2(\Sigma)$), which describe transitions from interband critical points in the joint density of states. Rakic and Majewski[26] proposed a modification model, in which the damping constants were replaced with the frequency dependent damping expressions.

The E_0 and $E_0 + \Delta_0$ transitions in GaAs occur in the center (Γ point) of the Brillouin zone. The contribution of these gap transitions to the dielectric function is given by[27]

$$\epsilon_1(E) = AE_0^{-3/2}\left[f(X_0) + \frac{1}{2}\left(\frac{E_0}{E_0 + \Delta_0}\right)^{3/2} f(X_{0S})\right], \tag{7}$$

with

$$f(X) = X^{-2}[2 - \sqrt{1+X} - \sqrt{1-X}], \tag{8}$$

$$X_0 = \frac{E + i\Gamma_0}{E_0}, \quad X_{0s} = \frac{E + i\Gamma_0}{E_0 + \Delta_0}, \tag{9}$$

where A and Γ_0 are the strength and damping constants of the E_0 and $E_0 + \Delta_0$ transitions, respectively. The exciton effect at the E_0 and $E_0 + \Delta_0$ critical points can be neglected for GaAs.

The E_1 and $E_1 + \Delta_1$ transitions in GaAs occur at the L point in Brillouin zone. The contribution of this type of transition to the dielectric function is given by[27]

$$\epsilon_2(E) = -B_1 X_1^{-2}\ln\left(1 - X_1^2\right) - B_{1s}X_{1s}\ln\left(1 - X_{1s}^2\right), \tag{10}$$

with

$$X_1 = \frac{E + i\Gamma_1}{E_1}, \quad X_{1s} = \frac{E + i\Gamma_1}{E_1 + \Delta_1}, \tag{11}$$

where $B_1(B_{1s})$ and Γ_1 are the strengths and damping constants of the E_1 and $E_1 + \Delta_1$ transitions, respectively. Since the Coulomb-like interaction is always present between electrons and holes, an excitonic state should exist. The contribution of the Wannier-type excitons at E_1 and $E_1 + \Delta_1$ critical points to dielectric function can be given by[27]

$$\epsilon_3(E) = \sum_{n=1}^{\infty}\frac{1}{(2n-1)^3}\left(\frac{B_{1x}}{E_1 - \left[G_1/(2n-1)^2\right] - E - i\Gamma_1} + \frac{B_{2x}}{E_1 + \Delta_1 - \left[G_{1s}/(2n-1)^2\right] - E - i\Gamma_1}\right), \tag{12}$$

where B_{1x} (B_{2x}) and G_1 (G_{1s}) are the strengths and Rydberg energy of the E_1 and $E_1 + \Delta_1$ excitons, respectively. Here, it is assumed that $G_1 = G_{1s} = 0$.

The nature of the E_0', $E_2(X)$, and $E_2(\Sigma)$ transitions is more complicated. They do not correspond to a single, well-defined critical point. These critical points can be characterized by damped harmonic oscillators and written as[28]

$$\epsilon_4(E) = \sum_{j=2}^{4}\frac{f_j^2}{E_j^2 - E^2 - iE\Gamma_j}, \tag{13}$$

with $f_j = \sqrt{C_j E_j^2}$, where C and Γ_j are strengths and damping constants of the E_j (E_0', $E_2(X)$, and $E_2(\Sigma)$) transitions, respectively.

In the modification model, the damping constants Γ_i are replaced with the frequency dependent damping expression Γ_i' given by[26]

$$\Gamma_i' = \Gamma\left[-\beta\left(\frac{E - E_0}{\Gamma}\right)^2\right], \tag{14}$$

where the additional parameter β allows for a continuous linear change of the range from a purely Lorentzian (for $\beta = 0$) to nearly Gaussian (for $\beta = 0.3$) functional forms.

The optical dielectric function is obtained by summing over all the contributions as described earlier and replacing the damping constants Γ_i with the frequency dependent damping expression Γ_i', and written by

$$\epsilon(E) = \epsilon_\infty + \epsilon_1(E) + \epsilon_2(E) + \epsilon_3(E) + \epsilon_4(E), \tag{15}$$

where ϵ_∞ is the high-frequency dielectric constant containing the contribution of higher-lying transitions. The energy gaps E_0, $E_0 + \Delta_0$, E_1, $E_1 + \Delta_1$, E_0', $E_2(X)$, and $E_2(\Sigma)$ change with the temperature; thus, the optical constant is a function of temperature. We finally arrive at the temperature dependence of the optical absorption coefficient α and reflectively R by recalling, $\epsilon = (n + ik)^2$ and noting

$$\alpha = \frac{4\pi k}{\lambda}, \tag{16}$$

$$R = \left|\frac{1-n}{1+n}\right|^2. \tag{17}$$

2. Calculating the electron diffusion length in GaAs

The electron diffusion length L represents the average distance an electron can travel before recombining with a hole in the valence band. This factor is expressed as

$$L = \sqrt{D \cdot \tau}, \tag{18}$$

where D represent the electron diffusion constant, τ represents the electron lifetime and $1/\tau$ represents the electron recombination rate, as described in Sec. I. There are three types of recombination in GaAs: radiative recombination, Auger recombination, and Shockley-Read-Hall recombination. The recombination rate depends on the doping concentration and temperature—typical values of $1/\tau$ range from 10^9 to $10^{10}\,s^{-1}$ and were determined experimentally by measuring ESP and using Eq. (1) and calculations of the spin relaxation rates given by Eqs. (2)–(4).

The diffusion constant D is given by the Einstein–Smoluchowski relation

$$D = \frac{\mu k_B T}{e}, \tag{19}$$

where e is the electron charge, T is the absolute temperature, k_B is the Boltzmann's constant, and μ is the electron mobility that also depends on the temperature and doping concentration, and can be estimated by[29]

$$\mu = \mu_{min} + \frac{\left(\frac{300\text{K}}{T}\right)^{\theta_1} \mu_{max}(300\text{K}) - \mu_{min}}{1 + \left(\frac{N}{(T/300\text{K})^{\theta_2} N_{ref(300\,\text{K})}}\right)^{\gamma}}, \tag{20}$$

where N is the doping concentration of GaAs; $\theta_1, \theta_2,$ and γ are constants; μ_{min} is the saturation mobility at a very high doping concentration, which is temperature independent; $\mu_{\max}(T)$ is the saturation mobility at a very low doping concentration, which itself reduces with increasing temperature; $N_{ref}(T) = \left(\frac{T}{300\,\text{K}}\right)^{\theta_2} N_{ref}(300\,\text{K})$ is the doping concentration at which mobility reduces to almost half of its maximum value at low doping.

To summarize, estimates of the spin relaxation rate for each sample can be made based on Eqs. (2)–(4). Then, together with the measurement of photocathode ESP versus illumination wavelength, the electron recombination rate can be inferred. From measurements of QE, the wavelength-dependent quantities R, α, and L, can be determined, which provide a means to calculate the photocathode escape probability, P_{esc}. Finally, in this paper, we attempt to correlate P_{esc} to ESP.

III. EXPERIMENT AND RESULTS

A. Experiment

All of the p-doped bulk GaAs samples were purchased from a commercial vendor and manufactured using the vertical gradient freeze technique. Sample characteristics, including Zn dopant carrier concentration and surface cleave plane orientation, are shown in Table I. Samples were cleaved into 15 × 15 mm squares from 3 in. diameter wafers. No chemical preparation was performed on samples prior to installation in the vacuum test chamber.

Each sample (one at a time) was attached to a sample holder and installed into an ultrahigh vacuum chamber with a low-voltage retarding-field Mott polarimeter.[30,31] A load-locked design necessitated that only a relatively small portion of the apparatus was baked each time a new sample was evaluated. The sample loading portion of the vacuum chamber was baked at 250 °C for 24 h and allowed to cool to room temperature. At typical vacuum pressure of $\sim 10^{-11}$ Torr was achieved following the bakeout. After chamber bakeout, the photocathode sample was lowered into position from which electrons could be extracted and delivered to the Mott scattering target. The sample was heated to 550 °C to remove adsorbed gas, then cooled to room temperature and activated to achieve a negative electron affinity condition using the standard yo-yo activation procedure[32] with cesium and NF_3. A broadly tunable super-continuum light source (NKT Photonics) provided up to milli-Watts of output power over wavelength range from 500 to 850 nm. The wavelength tunable light source emits picosecond pulses: light at low average power ($\sim\mu$W) was used to measure QE and ESP to avoid photoemission in a surface-charge-limited regime.[33,34] Optical waveplates (quarter and halfwave) were used to generate left and right circularly polarized light required to obtain spin polarized electrons.

The sample holder consisted of a hollow stainless steel tube with thin molybdenum end plate upon which the sample was affixed. The sample holder was designed to accommodate a heater, but also served as a cryostat when the heater was removed. For these measurements, the sample holder was filled with dry ice (frozen CO_2) or liquid nitrogen (LN_2). The substrate remained cold for many hours with just one filling. An assessment of the thermal resistance of the sample holder and the radiative heating from the vacuum chamber walls indicated that the substrate temperature was nearly identical to the temperature of the frozen CO_2 or LN_2.

B. Temperature and Zn dopant dependence

Three photocathodes, each with 100 surface cleave planes but with dopant densities spanning roughly 1.5 orders of magnitude, were activated at room temperature and evaluated using the retarding field Mott-polarimeter apparatus. Photocathode QE and ESP were measured as a function of

TABLE I. Specifications of the p-doped bulk GaAs samples.

Cleave plane	(111A)	(110)	(100)	(100)	(100)
Dopant	GaAs-Zn	GaAs-Zn	GaAs-Zn	GaAs-Zn	GaAs-Zn
Orientation	(111A) ± 0.5°	(110) ± 0.5°	(100) ± 0.5°	(100) ± 0.5°	(100) ± 0.5°
Carrier concentration (a./c.c.)	$1.1–1.14 \times 10^{19}$	$1.3–1.4 \times 10^{19}$	$1.0–1.3 \times 10^{19}$	$1.6–1.79 \times 10^{18}$	$5.01–6.0 \times 10^{17}$
Resistivity (Ω cm)	$7.17–7.38 \times 10^{-3}$	$6.1–6.6 \times 10^{-3}$	$6.6–7.7 \times 10^{-3}$	$2.48–2.68 \times 10^{-2}$	$5.4–6.23 \times 10^{-2}$
Mobility ($cm^2/V\,s$)	77–78	71–74	74–80	141–146	193–200
Thickness (μm)	500–550	475–525	600–650	325–375	425–475

illumination wavelength, first at room temperature and then with the sample holder filled with dry ice (195 K) and LN_2 (77 K). Care was taken to evaluate ESP at the same photocurrent to ensure similar photoelectron density at the photocathode, and at low laser power to minimize sensitivity to surface charge limit.

The QE and ESP spectral scans presented in Fig. 4 exhibit the typical shape for bulk GaAs, namely, ESP increases while QE decreases as the energy (wavelength) of the illumination light is decreased (increased), with the highest polarization obtained when the energy of the light is equal to the semiconductor bandgap ensuring that only electrons from the $P_{3/2}$ ground state are excited to the conduction band. More interesting is the effect of dopant density on QE and ESP. Higher dopant concentrations serve to increase band bending, which lowers the surface work function, which increases the electron escape probability and leads to higher QE, however, at the expense of polarization. For the commonly used dopant density of $10^{19}\,cm^{-3}$, photocathode QE at room temperature reached ~6.9% but provided a maximum ESP of only ~30%. Polarization increased to ~41% for the low-doped sample but provided QE of only ~1.5%. This behavior is consistent with predictions of the BAP mechanism that describes the spin relaxation rate proportional to the dopant concentration. Higher dopant concentration leads to greater spin relaxation rate, and thus lower ESP.

Cooling the samples to 77 K modifies the crystal lattice structure and shifts the bandgap energy.[35] This bandgap shift means peak polarization occurs at higher photon energies. The bandgap energy for GaAs can be calculated using $E_g(T) = 1.519\,\text{eV} - \frac{5.41\times10^{-4}T^2}{T+204\,\text{K}}$, which yields bandgaps of 1.51 and 1.42 eV for samples at 77 and 300 K, respectively. Only the 77 K bandgap "knee" is visible in the QE spectral plot of Fig. 4 (top right). More noteworthy is the significant increase in ESP observed for all three samples cooled to 77 K. The ESP for the highly doped sample increased from ~30% to 41%, and from ~40% to 52% for the low-doped sample. This behavior is consistent with Fig. 3 which predicts smaller spin relaxation rates for both mechanisms (BAP and DP) at lower temperature. It is interesting to note that for the low-doped sample at 77 K, measured polarization exceeds the theoretical maximum value of 50%. This could point to an inaccurate effective Sherman Function used in the Mott polarimeter analysis, with this measurement serving to identify the magnitude of systematic error relevant to the entire study, or perhaps an indication of interesting physics phenomenon, e.g., the creation of strain within the sample at cryogenic temperature, which serves to eliminate the energy level degeneracy of the $P_{3/2}$ ground state.

The temperature and dopant density studies are summarized in Fig. 5 (top), which shows the maximum ESP versus temperature for the three samples with different dopant concentrations. Fits were applied to the data sets based on Eq. (1), providing a means to determine the ratio of the electron recombination rate to the spin relaxation rate, τ/τ_s. The fit to the high dopant sample set is quite good, and less so for the lower dopant density results, although the fits still support the basic predicted trend, namely, lower temperature leads to lower spin relaxation rate and higher ESP. Figure 5 (bottom) shows the calculated spin relaxation rate based on Eqs. (2)–(4). A comparison to Fig. 3 indicates the BAP depolarization process dominates for all photocathode samples tests.

As mentioned earlier, sample temperature affects the bandgap energy, which influences the wavelength required for peak polarization. For a constant illumination wavelength, the QE of the photocathode decreases as the sample temperature is reduced. However, if the illumination wavelength is allowed to vary to achieve the highest ESP, photocathode QE should remain nearly constant. It was difficult to verify this statement because of surface contamination on the photocathode surface that occurred as samples were cooled to cryogenic temperature. Imperfect vacuum led to gas adsorption on the photocathode surface, which influenced P_{esc} and therefore QE. It was difficult to ensure identical photocathode surface conditions throughout the temperature study. The QE values for samples at room temperature, at the wavelength of peak

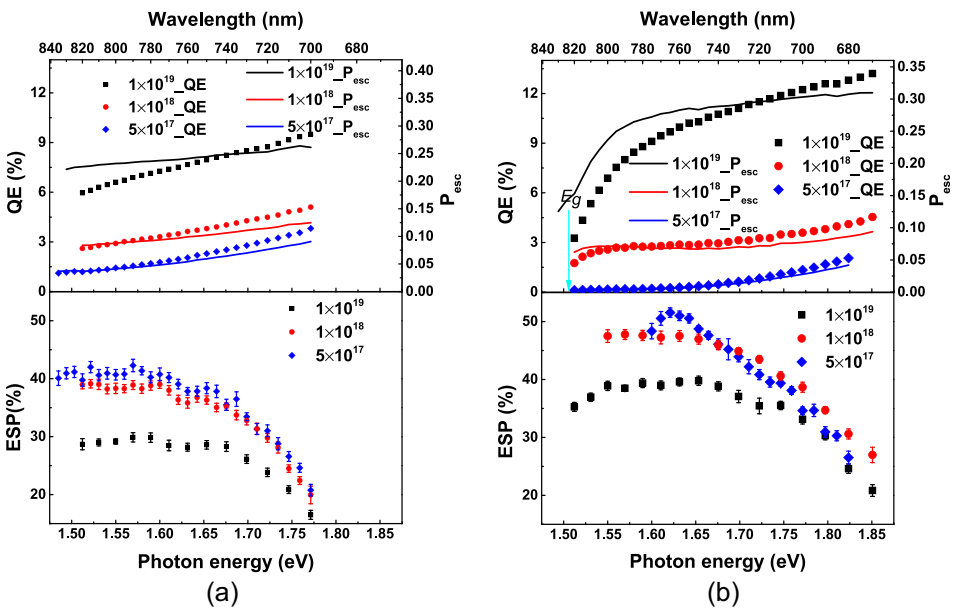

FIG. 4. The QE and ESP of bulk GaAs (100 cleave plane) with different Zn dopant densities, and measured at 300 K (left) and 77 K (right). Error bars are statistical. Axes ranges were kept identical to highlight the measurement variations observed between conditions. The bandgap energy E_g could be discerned for samples at 77 K (note arrow). The plots of escape probability P_{esc} are based on measured values of QE, and inferred values of reflectivity, absorption coefficient, and electron diffusion length as described in Sec. II.

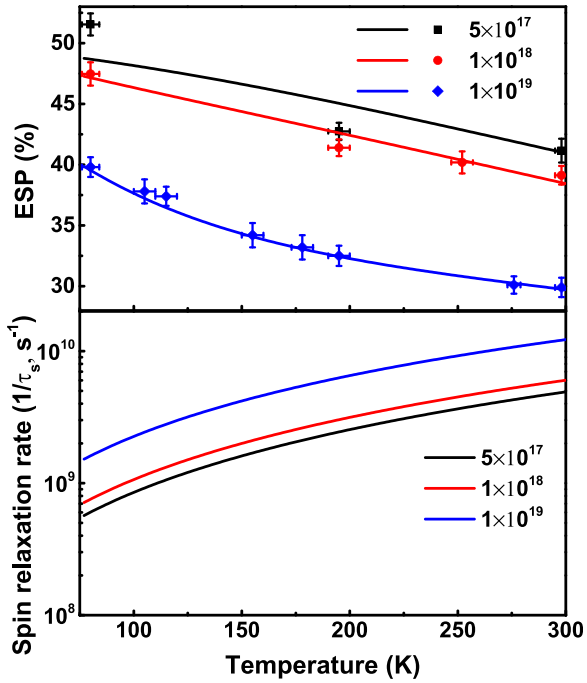

FIG. 5. (Top) Maximum ESP versus sample temperature and dopant density (the wavelength of illumination was allowed to vary to provide peak polarization). Dots are experimental data and lines represent fits based on calculations using Eqs. (2)–(4). Vertical error bars are statistical. Horizontal error bars are attributed to uncertainty in sample temperature. (Bottom) Calculated values of spin relaxation rate versus sample temperature and dopant density.

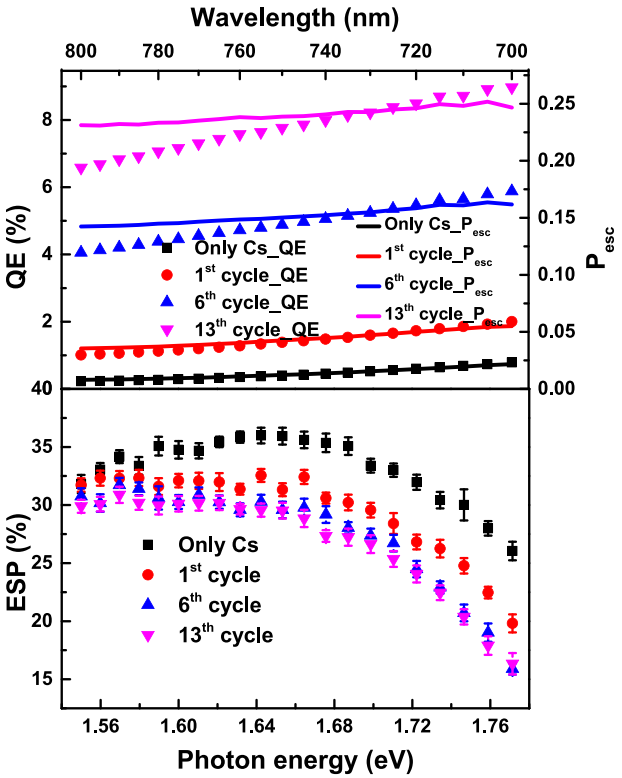

FIG. 6. QE, escape probability, and ESP for bulk GaAs (110 cleave plane) with dopant concentration of 1×10^{19} cm^{-3} as a function of surface activation layer. Cycle number refers to the number of applications of Cs and F. Error bars are statistical. The plots of escape probability P_{esc} are based on measured values of QE, and inferred values of reflectivity, absorption coefficient, and electron diffusion length as described in Sec. II.

polarization, were 6.9%, 3.1%, and 1.5% (in order decreasing dopant concentration) compared to 10%, 2.9%, and 0.79% for samples at 77 K.

C. Activation layer dependence

Some accelerators report delivering electron beams with higher ESP by intentionally varying the amount of chemicals applied to the photocathode surface[36] (i.e., the chemicals used to reduce the surface work function and create an NEA condition). To explore this behavior, the QE and ESP of GaAs photocathode with dopant concentration of 1×10^{19} cm^{-3} were measured at different times throughout the activation process. The so called "yo-yo" method of activation was employed, where the photocathode was exposed to incremental doses of Cs and NF_3 in an alternating manner until photocurrent (and therefore QE) reached a maximum value. The first measurements of QE and ESP occurred with only Cs deposited on the photocathode surface. Specifically, Cs was deposited until photocurrent fell to half of its first peak value. Then, QE and ESP were measured after adding only one dose of NF_3 which served to double the photocathode QE. Then, continuing the yo-yo activation, QE and ESP measurements were made at the 6th and 13th cycles. At the 13th application of Cs and NF_3, the photocathode QE had reached a maximum and the activation was considered complete. These measurements are summarized in Fig. 6, showing QE and ESP as a function of the photon energy and laser wavelength. The QE behavior is not surprising, with QE increasing significantly throughout the activation process until the photocathode NEA layer was fully formed at the 13th cycle. Photocathode QE at the wavelength of maximum polarization increased from 0.2, to 1.1, to 4.2% to 7%, for each of the cycles mentioned earlier. With only Cs, the maximum ESP was ~36% but fell to 32% with the addition of NF_3. At the 6th and 13th yo-yo cycles, ESP was constant at ~30%, which is a value consistent with measurements of the highly doped sample at room temperature described previously.

Reference 36 describes depolarization at the surface activation layer (Cs-O-Cs layer) governed by the functional form: $P(n) = P_0\exp(-\sigma n)$, where P_0 is the polarization of electrons that reached the photocathode surface but not passed through the activation layer, σ is the exchange scattering cross section between the electrons and the scattering sites in the activation layer, and n is the number of scatterers per cm^2 in the activation layer. This simple model suggests thicker activation layers introduce more scattering sites, and therefore more opportunity for spin relaxation. Our measurements partially support this idea, namely, an activation layer composed of only Cs provided the fewest scattering sites and the highest ESP. However, it would seem ESP would continue to decrease with each successive yo-yo cycle, whereas our measurements show nearly constant ESP for the 6th and 13th yo-yo cycles. This would imply there is a critical value of depolarization caused by this proposed mechanism. Once the thickness of a Cs-F layer reaches the critical value, additional Cs and NF_3 deposition does not lead to further depolarization.

Another explanation for the ESP behavior illustrated in Fig. 6 relates to the height of the surface work function, the width of the band bending region, and the thickness of the potential barrier that electrons must tunnel through to reach vacuum. When the NEA layer is fully formed, the height of the potential barrier is comparatively low, and the band bending region is wide. Electrons fall into the band bending region and thermalize. These electrons have more opportunity to depolarize and still leave the photocathode into vacuum. When the NEA layer is only partially formed, only the highest energy electrons can overcome the potential barrier at the surface, and these electrons have not thermalized, and therefore, they possess higher ESP.

D. Cleave planes dependence

The final study relates to the photocathode crystal orientation. Photocathode QE and ESP were evaluated for bulk GaAs samples with (100), (110), and (111A) surface cleave planes. Each sample had the same nominal Zn dopant concentration of 1×10^{19} cm^{-3}. Photocathodes were activated in an identical manner to ensure similar surface conditions. As shown in Fig. 7, the cleave planes (100) and (110) provided the highest QE (~7%) and cleave plane (111A) provided the lowest QE (~6%) at the wavelength of maximum polarization. No difference in ESP could be discerned between samples: the maximum ESP for all three samples was ~30%. From this measurement, it appears crystal orientation does not affect the ESP of bulk GaAs photocathodes.

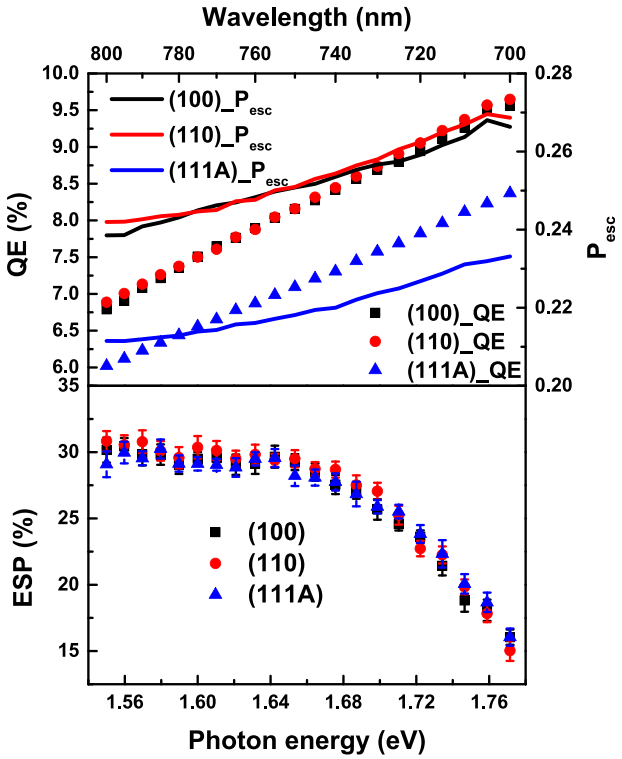

FIG. 7. QE, escape probability, and ESP of bulk GaAs with three different cleave planes, Zn dopant concentration of 1×10^{19} cm^{-3} measured at room temperature. Error bars are statistical. The plots of escape probability P_{esc} are based on measured values of QE, and inferred values of reflectivity, absorption coefficient, and electron diffusion length as described in Sec. II.

IV. DISCUSSION

This work clearly illustrates the importance of temperature and dopant density as factors that influence ESP of bulk GaAs photocathodes, in a manner consistent with accepted BAP and DP spin relaxation mechanisms. Highly doped bulk GaAs samples at room temperature provide ESP ~ 30%, but at low temperature and with low dopant concentration, samples provided ESP comparable to the theoretical maximum value of 50%. Measured ESP of 52% (for lowest doped sample at 77 K) could indicate an inaccurate effective Sherman Function used in the Mott polarimeter analysis, however the retarding field Mott polarimeter was originally calibrated against the MeV Mott polarimeter used at CEBAF,[37] which is considered to be a very accurate device. Table II lists maximum ESP values from cited references. Maximum ESP values exceeding 50% from bulk GaAs were also reported by Pierce and Meier[8] Our dopant density-dependent measurements contradict those of Fishman and Lampel[17] who reported increasing ESP as at higher dopant concentration. However, it is widely accepted that higher ESP is obtained with lower dopant concentrations—these older measurements must have suffered from an unknown systematic error.

Our measurements also point to ESP sensitivity to the activation layer. A photocathode with a more fully formed NEA condition, i.e., a thicker activation layer, exhibited lower ESP. Two explanations were discussed: electron scattering within the Cs-F surface layer, and a filtering effect associated with the characteristics of the band bending region. Because measured ESP was only sensitive to the first yo-yo cycles of chemical deposition, it seems more likely the observed ESP dependence relates to the characteristics of the band bending region. A thicker activation layer reduces the work function at the surface, creating a deeper band

TABLE II. Reported maximum ESP values.

References	Note	Dopant concentration (cm^{-3})	Temperature (K)	Max ESP (%)
This work		1×10^{19}	300	30
This work		1×10^{19}	77	40
This work		$5–6 \times 10^{17}$	77	52
Ref. 8 (Pierce)	NEA	1.3×10^{19}	<10	40
Ref. 8 (Pierce)	PEA	1.3×10^{19}	<10	54
Ref. 21 (Maruyama)	0.9 μm thick	5×10^{18}	300	41
Ref. 21 (Maruyama)	0.2 μm thick	5×10^{18}	300	49
Ref. 17 (Fishman)		4×10^{19}	4.2	45
Ref. 17 (Fishman)		4×10^{18}	4.2	41
Ref. 17 (Fishman)		8×10^{16}	4.2	38
Ref. 17 (Fishman)		4×10^{18}	77	29
Ref. 38 (Hartmann)	Time resolved – Max. value	$2–3 \times 10^{19}$	300	43
Ref. 38 (Hartmann)	Time resolved - Ave. value	$2–3 \times 10^{19}$	300	27

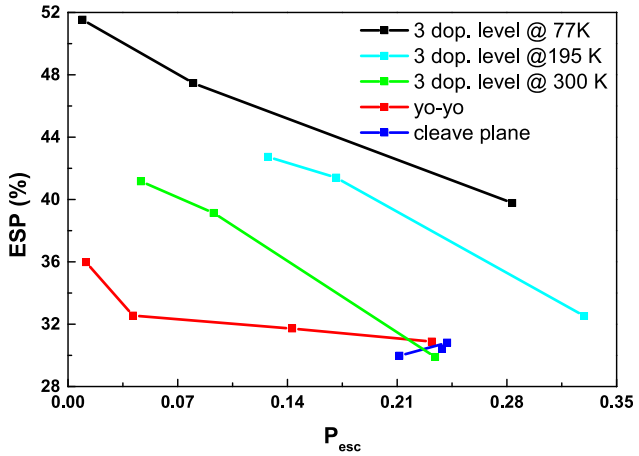

FIG. 8. Maximum ESP versus P_{esc} for all of the bulk GaAs photocathodes studied.

bending region. Electrons thermalize within the band bending region, with more opportunity to depolarize, and yet still escape to vacuum. A thinner activation layer provides a comparatively higher potential barrier which serves to filter out electrons that have suffered depolarization. This measured trend is consistent with the measurements of Ref. 8, comparing positive and negative electron affinity surface conditions.

Although cleave plane samples (100) and (110) provided higher QE compared to cleave plane (111A), there was no ESP sensitivity to crystal orientation.

In the introductory sections of this paper, considerable effort was devoted to deriving P_{esc} with the intention of discerning a relationship between P_{esc} and ESP. The QE and ESP measurements presented herein where used to infer values of reflectivity, absorption coefficient, and electron diffusion length. In turn these values allowed for calculation of P_{esc} with accompanying plots included in Figs. 4, 6, and 7 and summarized in Fig. 8, which shows maximum EPS versus P_{esc}. With the exception of "cleave plane," all of the parametric variables studied show ESP inversely proportional to P_{esc}, and consequently QE. So, in general, it can be said that ESP can be increased at the expense of QE. But it is also important to note low QE does not always imply high ESP. For example, a photocathode with contaminated surface can provide both low QE and low ESP.

ACKNOWLEDGMENTS

Authored by Jefferson Science Associates under U.S. DOE Contract No. DE-AC05-06OR23177. The U.S. Government retains a non-exclusive, paid-up, irrevocable, world-wide license to publish or reproduce this manuscript for U.S. Government purposes.

[1]R. Alley, H. Aoyagi, J. Clendenin, J. Frisch, C. Garden, E. Hoyt, R. Kirby, L. Klaisner, A. Kulikov, R. Miller *et al.*, Nucl. Instrum. Methods, A **365**(1), 1 (1995).
[2]K. Aulenbacher, C. Nachtigall, H. G. Andresen, J. Bermuth, T. Dombo, P. Drescher, H. Euteneuer, H. Fischer, D. V. Harrach, P. Hartmann *et al.*, Nucl. Instrum. Methods, A **391**, 498 (1997).
[3]C. K. Sinclair, P. A. Adderley, B. M. Dunham, J. C. Hansknecht, P. Hartmann, M. Poelker, J. S. Price, P. M. Rutt, W. J. Schneider, and M. Steigerwald, Phys. Rev. ST Accel. Beams **10**, 023501 (2007).
[4]J. Smedley, E. Muller, and D. Dimitrov, private communication (2016).
[5]D. Abbott, P. Adderley, A. Adeyemi, P. Aguilera, M. Ali, H. Areti, M. Baylac, J. Benesch, G. Bosson, B. Cade *et al.*, Phys. Rev. Lett. **116**, 214801 (2016).
[6]E. C. Aschenauer, M. D. Baker, A. Bazilevsky, K. Boyle, S. Belomestnykh, I. Ben-Zvi, S. Brooks, C. Brutus, T. Burton, S. Fazio *et al.*, e-print arXiv:1409.1633.
[7]J. S. Blakemore, J. Appl. Phys. **53**, R123 (1982).
[8]D. T. Pierce and F. Meier, Phys. Rev. B **13**, 5484 (1976).
[9]W. E. Spicer, Phys. Rev. **112**, 114 (1958).
[10]L. W. James, G. A. Antypas, J. Edgecumbe, R. L. Moon, and R. L. Bell, J. Appl. Phys. **42**, 4976 (1971).
[11]M. I. D'yakonov and V. I. Perel, Zh. Eksp. Teor. Fiz. **60**, 1954 (1971) [Sov. Phys. - JETP **33**, 1053 (1971) (in Russian)].
[12]G. L. Bir, A. G. Aronov, and G. E. Pikus, Zh. Eksp. Teor. Fiz. **69**, 1382 (1975) [Sov. Phys. - JETP **42**, 705 (1975) (in Russian)].
[13]F. Meier and B. P. Zakharchenya, *Optical Orientation* (North-Holland Physics, Netherlands, 1984), pp.108–129.
[14]P. H. Song and K. W. Kim, Phys. Rev. B **66**, 035207 (2002).
[15]R. J. Elliot, Phys. Rev. **96**, 266 (1954).
[16]Y. Yafet, in *Solid State Physics*, edited by F. Seitz and D. Turnbull (Academic Press, New York, 1963), Vol. 14, pp. 1–98.
[17]G. Fishman and G. Lampel, Phys. Rev. B **16**, 820 (1977).
[18]A. G. Aronov, G. E. Pikus, and A. N. Titkov, Sov. Phys. - JETP **57**, 680 (1983); available at http://www.jetp.ac.ru/cgi-bin/e/index/e/57/3/p680?a=list.
[19]K. Zerrouati, F. Fabre, G. Bacquet, J. Bandet, J. Frandon, G. Lampel, and D. Paget, Phys. Rev. B **37**, 1334 (1988).
[20]J. H. Jiang and M. W. Wu, Phys. Rev. B **79**, 125206 (2009).
[21]T. Maruyama, R. Prepost, E. L. Garwin, C. K. Sinclair, B. Dunham, and S. Kalem, Appl. Phys. Lett. **55**, 1686 (1989).
[22]I. Zutic, J. Fabian, and S. Das Sarma, Rev. Mod. Phys. **76**, 323 (2004).
[23]W. E. Spicer and A. Herrera-Gómez, "Modern theory and applications of photocathodes," Proc. SPIE **2022** (1993).
[24]S. Adachi, J. Appl. Phys. **53**, 5863 (1982).
[25]S. Adachi, J. Appl. Phys. **58**, R1 (1985).
[26]A. D. Rakic and M. L. Majewski, J. Appl. Phys. **80**, 5909 (1996).
[27]S. Ozaki and S. Adachi, J. Appl. Phys. **78**, 3380 (1995).
[28]A. B. Djurišić, A. D. Rakić, P. C. K. Kwok, E. H. Li, M. L. Majewski, and J. M. Elazar, J. Appl. Phys. **86**, 445 (1999).
[29]M. Sotoodeh, A. H. Khalid, and A. A. Rezazadeh, J. Appl. Phys. **87**, 2890 (2000).
[30]J. L. McCarter, M. L. Stutzman, K. W. Trantham, T. G. Anderson, A. M. Cook, and T. J. Gay, Nucl. Instrum. Methods, A **618**, 30 (2010).
[31]J. L. McCarter, A. Afanasev, T. J. Gay, J. Hansknecht, A. Kechiantz, and M. Poelker, Nucl. Instr. Methods, A **738**, 149 (2014).
[32]R. L. Bell, *Negative Electron Affinity Devices* (Clarendon Press, Oxford, England, 1973).
[33]M. Woods, J. Clendenin, J. Frisch, A. Kulikov, P. Saez, D. Schultz, J. Turner, K. Witte, and M. Zolotorev, J. Appl. Phys. **73**, 8531 (1993).
[34]P. J. Saez, "Polarization and charge limit studies of strained GaAs photocathodes," Ph. D. thesis (Stanford University, 1997).
[35]B. V. Zeghbroeck, see http://ecee.colorado.edu/~bart/book/book/contents.htm for Principles of semiconductor devices (2011), Chap. 2.
[36]M. Erbudak and B. Reihl, Appl. Phys. Lett. **33**, 584 (1978).
[37]M. Steigerwald, "MeV Mott Polarimetry at Jefferson Lab," AIP Conf. Proc. **570**, 935 (2001).
[38]P. Hartmann, "Aufbau einer gepulsten Quelle polarisierter Elektronen," Ph.D. Dissertation (Shaker Verlag, Aachen, 1998).